materials

MDPI

Article

Boosting the Dehydrogenation Properties of $LiAlH_4$ by Addition of $TiSiO_4$

Nurul Yasmeen Yusnizam, Nurul Amirah Ali, Noratiqah Sazelee and Mohammad Ismail *

Energy Storage Research Group, Faculty of Ocean Engineering Technology and Informatics, Universiti Malaysia Terengganu, Kuala Nerus 21030, Malaysia; nurulyasmeen.yusnizam@gmail.com (N.Y.Y.); nurulllamirah@gmail.com (N.A.A.); atiqahsazelee19@gmail.com (N.S.)

* Correspondence: mohammadismail@umt.edu.my; Tel.: +60-9-6683487

Abstract: Given its significant gravimetric hydrogen capacity advantage, lithium alanate ($LiAlH_4$) is regarded as a suitable material for solid-state hydrogen storage. Nevertheless, its outrageous decomposition temperature and slow sorption kinetics hinder its application as a solid-state hydrogen storage material. This research's objective is to investigate how the addition of titanium silicate ($TiSiO_4$) altered the dehydrogenation behavior of $LiAlH_4$. The $LiAlH_4$–10 wt% $TiSiO_4$ composite dehydrogenation temperatures were lowered to 92 °C (first-step reaction) and 128 °C (second-step reaction). According to dehydrogenation kinetic analysis, the $TiSiO_4$-added $LiAlH_4$ composite was able to liberate more hydrogen (about 6.0 wt%) than the undoped $LiAlH_4$ composite (less than 1.0 wt%) at 90 °C for 2 h. After the addition of $TiSiO_4$, the activation energies for hydrogen to liberate from $LiAlH_4$ were lowered. Based on the Kissinger equation, the activation energies for hydrogen liberation for the two-step dehydrogenation of post-milled $LiAlH_4$ were 103 and 115 kJ/mol, respectively. After milling $LiAlH_4$ with 10 wt% $TiSiO_4$, the activation energies were reduced to 68 and 77 kJ/mol, respectively. Additionally, the scanning electron microscopy images demonstrated that the $LiAlH_4$ particles shrank and barely aggregated when 10 wt% of $TiSiO_4$ was added. According to the X-ray diffraction results, $TiSiO_4$ had a significant effect by lowering the decomposition temperature and increasing the rate of dehydrogenation of $LiAlH_4$ via the new active species of AlTi and Si-containing that formed during the heating process.

Keywords: $LiAlH_4$; $TiSiO_4$; hydrogen storage; dehydrogenation properties

check for updates

Citation: Yusnizam, N.Y.; Ali, N.A.; Sazelee, N.; Ismail, M. Boosting the Dehydrogenation Properties of $LiAlH_4$ by Addition of $TiSiO_4$. *Materials* **2023**, *16*, 2178. https://doi.org/10.3390/ma16062178

Academic Editors: Alessandro Dell'Era and Erwin Ciro Zuleta

Received: 7 February 2023
Revised: 21 February 2023
Accepted: 23 February 2023
Published: 8 March 2023

Copyright: © 2023 by the authors. Licensee MDPI, Basel, Switzerland. This article is an open access article distributed under the terms and conditions of the Creative Commons Attribution (CC BY) license (https://creativecommons.org/licenses/by/4.0/).

1. Introduction

Concerns about the energy crisis and the environment have led to an increase in the proportion of renewable energy sources in the energy system, such as wind, hydro, and other types. The supply and utilization times are typically out of sync and have some geographical restrictions. The proper secondary energy must be selected to match them, and hydrogen is a promising alternative to meet the demands for clean and sustainable energy technologies [1]. Hydrogen energy is a perfect substitute for petroleum because of its high energy density and lack of carbon emissions [2–7].

Hydrogen can be stored in a variety of ways for application purposes. As of now, compressed gas has been the most popular technique. It can also be kept as a liquid at extremely low temperatures. Other methods of storing hydrogen are via the solid-state method through physisorption and chemisorption [8]. Storing hydrogen via the solid-state method is regarded as the most promising method. Based on the US Department of Energy (DOE), by 2025, the fuel cell materials should store 5.5 wt% (gravimetric) and 40 g L^{-1} (volumetric) of hydrogen [9]. Complex hydride has emerged as the most promising medium for solid-state hydrogen storage based on the DOE target due to its high hydrogen storage capacity. Additionally, based on previous research, storing hydrogen is promising in metal or complex hydrides via chemisorption. This technique involves absorbing and storing

hydrogen in a metal powder made of either pure metal or an alloy. The metal/complex hydride material generates heat when hydrogen is absorbed into it, and heat is required for the metal/complex hydride to generate hydrogen again. As a result of the hydrogen's strong bonding with the metal in some materials, it requires extreme temperatures, more than 400 °C for magnesium, as an example [10,11]. This is a disadvantage of the metal/complex hydride storage method [12–14]. Among metal or complex hydride materials, one of the best potential candidates is said to be lithium alanate ($LiAlH_4$) [15–20]. $LiAlH_4$ is thought to be a promising material for storing hydrogen in solid-state form as it has a greater capacity to store hydrogen compared to other complex hydrides. Table 1 compares the properties of $LiAlH_4$ with other complex hydrides.

Table 1. Properties of $LiAlH_4$ and other complex hydrides [21–25].

Materials	Cost of Material ($ g^{-1})	Desorption Kinetics	Gravimetric (wt%)	Volumetric (g L^{-1})
$LiAlH_4$	3.7	~0.04 wt% (within 180 min, 90 °C)	10.5	96.7
$NaAlH_4$	10.8	~0.01 wt% (within 150 min, 140 °C)	7.4	94.8
KBH_4	1.41	NA	7.4	87.1
$NaNH_2$	6.19	NA	5.2	71.9

$LiAlH_4$ decomposes in three steps, as shown in Equations (1)–(3),

$$LiAlH_4 \rightarrow 1/3Li_3AlH_6 + 2/3Al + H_2 \text{ (about 5.3 wt\% of } H_2 \text{ liberated)} \quad (1)$$

$$Li_3AlH_6 \rightarrow 3LiH + Al + 3/2H_2 \text{ (about 2.6 wt\% of } H_2 \text{ liberated)} \quad (2)$$

$$LiH + Al \rightarrow LiAl + 1/2H_2 \text{ (about 2.6 wt\% of } H_2 \text{ liberated)} \quad (3)$$

However, its application is hampered by its high dehydrogenation temperature, slow dehydrogenation kinetics, and reversibility issues. According to previous studies [19,26–28], these challenges were addressed through several modifications, such as particle size reduction utilizing the ball milling method and doping with a catalyst. Some examples of doping with catalysts in the literature [19,29–35] include doping with metal halides, metal oxides, and carbon-based additives.

Complex metal oxide additives, especially secondary metal oxides, are a newly emerging research area to further enhance $LiAlH_4$'s dehydrogenation abilities [36–38]. The study of the catalysis of Al_2TiO_5 on the dehydrogenation properties of $LiAlH_4$ demonstrated that the onset temperatures dropped significantly after milling with 5 wt% Al_2TiO_5 [39]. The hydrogen began to be liberated at about 90 °C and 137 °C for both steps, respectively. Meanwhile, Zhai et al. [36] investigated how $MnFe_2O_4$ affected $LiAlH_4$'s dehydrogenation properties and discovered that the temperature at which decomposition began was about 70 °C lower than it would have been otherwise. Moreover, the research conducted by Ismail et al. [40] proved that the onset desorption temperature of the two stages of the $LiAlH_4$ was reduced to 80 °C and 120 °C, respectively, when doped with $SrTiO_3$, as opposed to the as-obtained $LiAlH_4$. The $LiAlH_4$ dehydrogenation kinetics were also enhanced as the $SrTiO_3$-doped $LiAlH_4$ composite could liberate about 3.0 wt% of hydrogen at 90 °C in 20 min as opposed to the undoped composite's 0.2 wt% in the same time frame.

However, more research is necessary to determine whether other secondary metal oxide-based catalysts could lower the decomposition temperature and improve $LiAlH_4$ dehydrogenation kinetic efficiency. In this study, we have used another secondary metal oxide to boost the dehydrogenation properties of $LiAlH_4$. To the best of our knowledge, no research has been conducted on enhancing $LiAlH_4$'s ability to store hydrogen using $TiSiO_4$ as a catalyst.

2. Materials and Methods

Sigma Aldrich (Burlington, MA, USA) provided $LiAlH_4$ (purity 95.0%) and $TiSiO_4$ (purity 99.8%) powders that were used without any changes. Every stage of the sample preparation process, including loading and weighing, was completed in an MBraun Unilab glove box to avoid oxidation. The sample ($LiAlH_4$ + 10 wt% $TiSiO_4$) was then directly milled in an NQM-0.4 planetary ball mill for 1 h (15 min milling, followed by three cycles of 2 min rest between rotations) at a rate of 400 rpm.

A Sievert-type apparatus (Advanced Materials Corporation, Pittsburgh, PA, USA) was used to study the onset dehydrogenation temperature and the kinetic property for the liberation of H_2 from the undoped $LiAlH_4$ and the $TiSiO_4$-added $LiAlH_4$ composite. The sample was heated from room temperature to 250 °C at a heating rate of 5 °C/min in a vacuum environment for the onset dehydrogenation temperature characterization. To determine the kinetics of H_2 liberation, the sample was heated at a constant temperature of 90 °C while being exposed to an H_2 pressure of 1.0 atm. Differential scanning calorimetry (DSC) from Setline STA: Simultaneous Thermal Analysis (SETARAM) was used to investigate the thermal properties of the samples. The DSC measurements were run at heating rates of 15 °C/min, 20 °C/min, 25 °C/min, and 30 °C/min. The argon gas flow rate was set to 50 mL/min, and the temperature range for this measurement was set to 300 °C. The microstructure of the sample before and after the milling process was examined using scanning electron microscopy (SEM; JEOL JSM 6360LA). The phase structure of the sample before and after the ball mill and after the dehydrogenation process was studied using an X-ray diffractometer (XRD, Rigaku Miniflex, Tokyo, Japan) and Fourier transform infrared (IR, Shimadzu Tracer-100, Tokyo, Japan).

3. Results and Discussion

Figure 1 depicts the results of the research on the onset thermal dehydrogenation and dehydrogenation kinetics processes for both added and undoped composites ($LiAlH_4$ and 10 wt% $TiSiO_4$ systems). Two distinguishing features of each composite's dehydrogenation reaction are shown on the graph. As shown in Figure 1a, at about 146 °C, the as-obtained $LiAlH_4$ has initiated the liberation of hydrogen, and further heating has led to the beginning of a second stage dehydrogenation process at about 180 °C. After 1 h of the $LiAlH_4$ milling process, the first and second steps' onset dehydrogenation temperatures drop to about 144 °C and 174 °C, respectively. This result demonstrates how the ball milling technique insignificantly influenced the dehydrogenation temperature of $LiAlH_4$. Moreover, doping 10 wt% of $TiSiO_4$ drastically lowered the decomposition temperatures for the two steps at 92 °C and 128 °C. Adding $TiSiO_4$ as a catalyst proved to enhance the dehydrogenation performance of $LiAlH_4$.

Figure 1b shows the isothermal dehydrogenation kinetics at 90 °C for doped and undoped samples. Less than 1.0 wt% of hydrogen was liberated in 80 min by the undoped sample. Under the same conditions, the hydrogen's liberate capacity increased significantly to 5.7 wt% after 10 wt% $TiSiO_4$ was added. As a result, the $TiSiO_4$-added $LiAlH_4$ sample desorbs at a rate that is, on average, 5 to 6 times higher than the undoped $LiAlH_4$. According to this result, the catalyst addition of $TiSiO_4$ improved the kinetics of $LiAlH_4$ dehydrogenation. The outcome shows that the kinetics of $LiAlH_4$ dehydrogenation were improved by the catalyst doping, as previous studies stated [15,41,42].

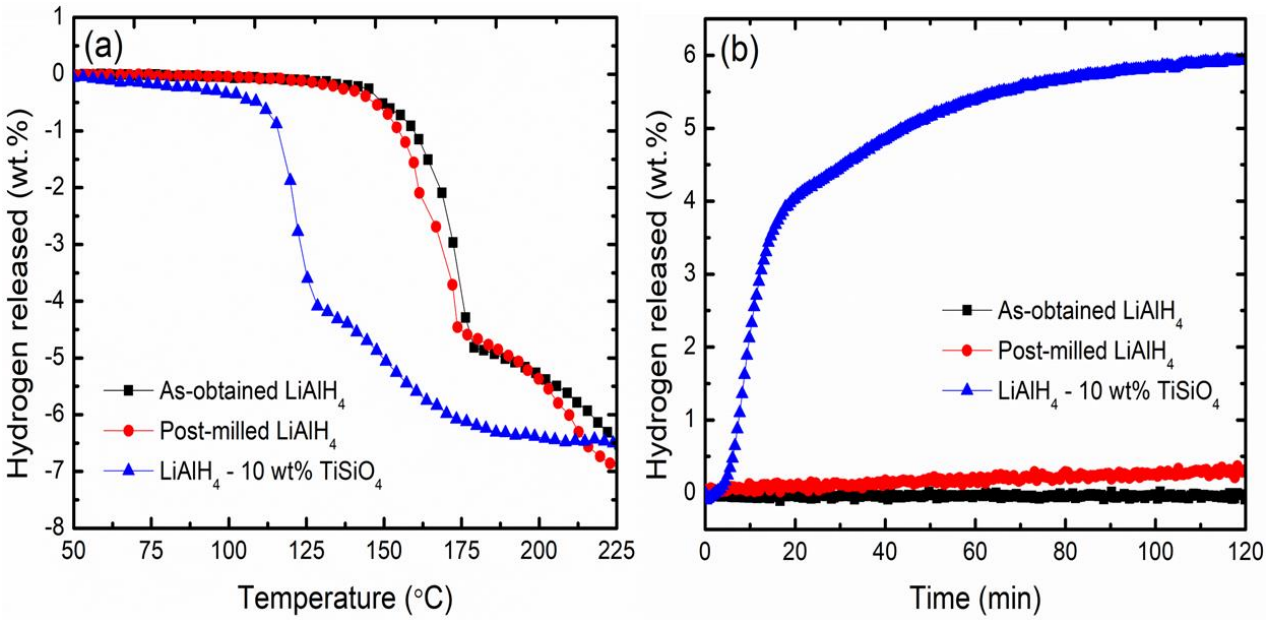

Figure 1. (**a**) TPD curve of as-obtained $LiAlH_4$, post-milled $LiAlH_4$, and $LiAlH_4$ added with 10 wt% $TiSiO_4$ at 250 °C and (**b**) the dehydrogenation kinetics performance at a constant temperature of 90 °C for the added and undoped composites.

The catalytic effects of $TiSiO_4$ on the thermal properties of $LiAlH_4$ were validated using DSC measurements on added and undoped $LiAlH_4$. Temperatures ranging from 25 °C to 300 °C, with an argon flow rate of 50 mL/min, were used for the investigation. Figure 2 displays the DSC curves for added and undoped $LiAlH_4$ at a rate of 15 °C/min. The thermal characteristics of as-obtained $LiAlH_4$ have four peaks. Two are exothermic, while the other two are endothermic. The interaction of hydroxyl impurities with $LiAlH_4$'s surface caused the first exothermic peak to appear at 150 °C, while the melting of $LiAlH_4$ caused the first endothermic peak to appear at 175 °C [37,40,43,44]. In the meantime, the dehydrogenation of liquid $LiAlH_4$ causes the second exothermic peak (190 °C). Li_3AlH_6 decomposition (265 °C) was responsible for the second endothermic peak. These second exothermic and endothermic peaks were assigned to Equations (1) and (2), respectively. These similar peaks also occurred to the post-milled $LiAlH_4$, but at lower temperatures.

The thermal event of $LiAlH_4$ is lowered from four to two after the addition of $TiSiO_4$. The exothermic event peak at around 120 °C seems to correspond to the decomposition of $LiAlH_4$ (Equation (1)), and the endothermic event peak at around 176 °C is most likely to correspond to the decomposition of Li_3AlH_6 (Equation (2)). The first endothermic event associated with $LiAlH_4$ melting has vanished from the DSC curve of $TiSiO_4$-doped $LiAlH_4$. The disappearance of the melting event is most likely owing to the fact that the decomposition temperature of the first stage of the doped sample is lower than the melting temperature of post-milled $LiAlH_4$.

Different heating rates were measured using DSC to examine the impact of $TiSiO_4$ addition on the activation energy (E_A) for hydrogen desorbed from $LiAlH_4$. The DSC curves for the added and undoped $LiAlH_4$ samples at various heating rates (15, 20, 25, and 30 °C/min) are shown in Figure 3a,b. The Kissinger equation used to calculate the E_A values of the dehydrogenation process of the 1 h milled $LiAlH_4$ and $LiAlH_4$–10 wt% $TiSiO_4$ composite is as follows:

$$\ln [\beta/T_p^2] = -E_A/RT_p + A \quad (4)$$

where R is the gas constant, A is a linear constant, T_p is the peak temperature on the DSC dehydrogenation curves, E_A is the activation energy, and β is the DSC heating rate.

Consequently, the E_A was determined using the graph's slope, ln $\left[\beta/T_p^2\right]$ vs. $1000/T_p$. The Kissinger plots for the dehydrogenation of $LiAlH_4$ (1st stage) and the dehydrogenation of Li_3AlH_6 (2nd stage) for both composites are shown in Figure 3c,d. Based on the slopes, E_A for the post-milled $LiAlH_4$ are 103 kJ/mol (1st stage dehydrogenation) and 115 kJ/mol (2nd stage dehydrogenation), respectively. Meanwhile, the E_A for the first and second stages of dehydrogenation, respectively, are reduced to 68 kJ/mol and 77 kJ/mol for the added system with 10 wt% $TiSiO_4$.

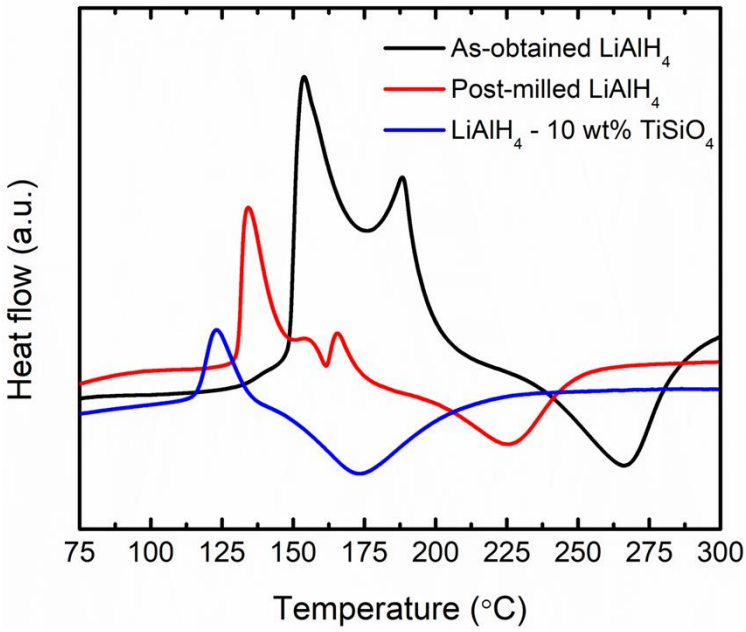

Figure 2. DSC data recorded at a rate of 15 °C/min for as-obtained $LiAlH_4$, post-milled $LiAlH_4$, and $LiAlH_4$ added with 10 wt% $TiSiO_4$.

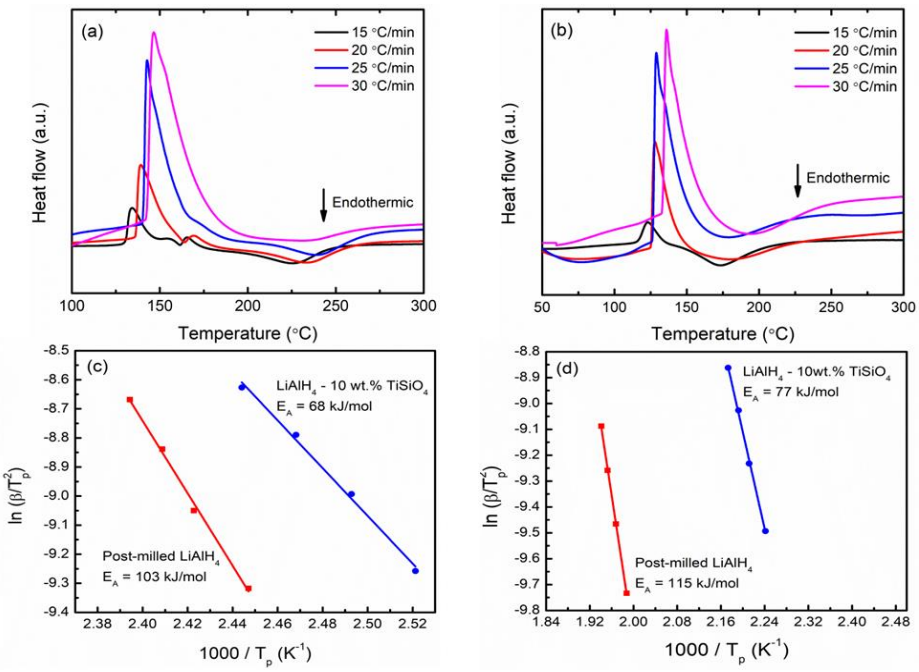

Figure 3. DSC dehydrogenation curves at different heating rates for (**a**) post-milled $LiAlH_4$, (**b**) $LiAlH_4$–10 wt% $TiSiO_4$ and Kissinger's plot for the (**c**) first and (**d**) second dehydrogenation stage of post-milled $LiAlH_4$ and $LiAlH_4$ added with 10 wt% $TiSiO_4$.

Figure 4 shows the morphology differences between the $TiSiO_4$, added, and undoped $LiAlH_4$ samples. Figure 4a shows the morphology for the as-obtained $TiSiO_4$, which is a fine particle. Figure 4b depicts the as-obtained $LiAlH_4$'s morphology, which is described as rough and asymmetrical in shape. The particle size of $LiAlH_4$ was smaller but aggregated and inhomogeneous after a 1 h milling process (Figure 4c). The particle size of the 10 wt% $TiSiO_4$-doped $LiAlH_4$ sample (Figure 4d) has shrunk and is less aggregated compared to post-milled $LiAlH_4$. The 10 wt% $TiSiO_4$-added $LiAlH_4$ composite has a larger surface area due to the smaller particle sizes. Previous research has shown that surface modification significantly improves the hydrogen storage properties of metals and complex hydride materials [34,45–47].

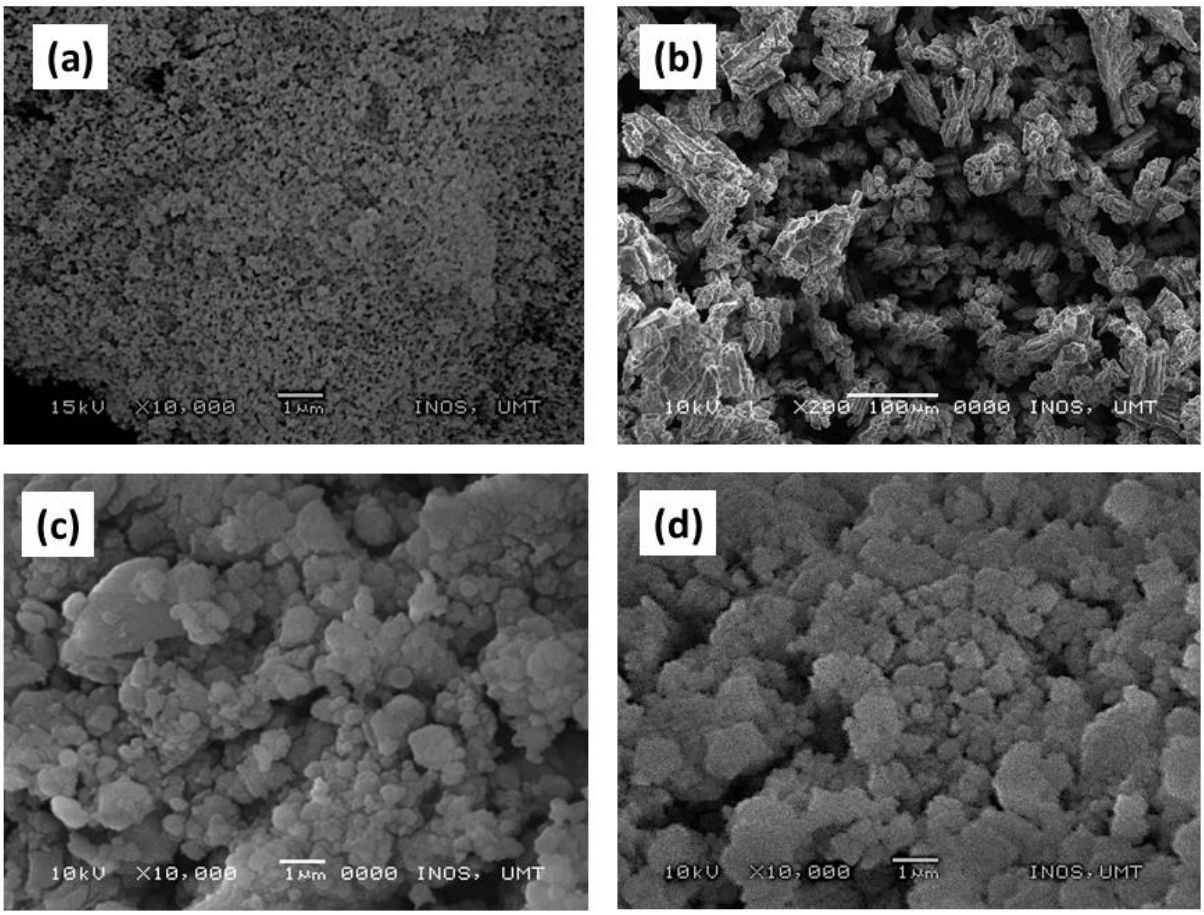

Figure 4. The morphological structures of (**a**) as-obtained $TiSiO_4$, (**b**) as-obtained $LiAlH_4$, (**c**) post-milled $LiAlH_4$, and (**d**) $LiAlH_4$ added with 10 wt% $TiSiO_4$.

The particle size distribution of the $TiSiO_4$, added, and undoped $LiAlH_4$ samples were determined using the Image J software, as demonstrated in Figure 5. Based on the histogram shown in Figure 5a–d, the estimated average particle sizes for the as-obtained $TiSiO_4$, as-obtained $LiAlH_4$, post-milled $LiAlH_4$, and $LiAlH_4$ added with 10 wt% $TiSiO_4$ were determined to be 6.10, 81.58, 61.71, and 28.13 μm, respectively. These findings demonstrated that the addition of 10 wt% $TiSiO_4$ to $LiAlH_4$ significantly reduced particle size. Previous studies by Ahmad et al. [22] and Cai et al. [48] stated the added $LiAlH_4$ increased the rate of hydrogen diffusion, which resulted in fast dehydrogenation kinetics and low activation energy. Additionally, its smaller particle size results in a larger surface area and more grain boundaries [36,38,49].

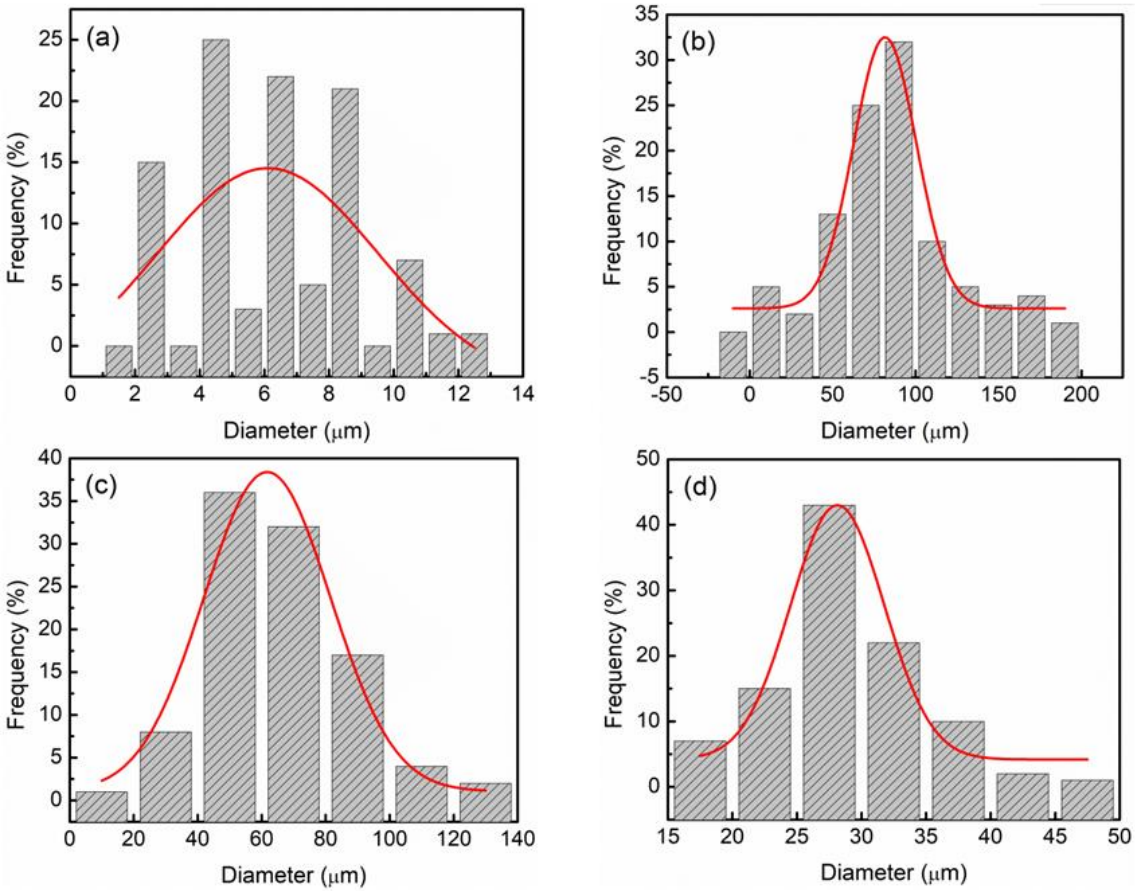

Figure 5. Particle size distribution histograms of the (**a**) as-obtained $TiSiO_4$, (**b**) as-obtained $LiAlH_4$, (**c**) post-milled $LiAlH_4$, and (**d**) $LiAlH_4$ added with 10 wt% $TiSiO_4$.

Figure 6 shows the XRD pattern of the as-obtained and post-milled $LiAlH_4$, $TiSiO_4$-doped $LiAlH_4$ composite, and as-obtained $TiSiO_4$ sample. The sample of as-obtained $TiSiO_4$ shows the high purity of $TiSiO_4$ [50]. For the as-obtained $LiAlH_4$ sample, as shown in Figure 6a, the peaks of $LiAlH_4$ are dominant, and there are no other peaks detected, proving that the as-obtained $LiAlH_4$ sample is pure, as stated by the supplier. Furthermore, as shown in Figure 6b, even after the ball milling process of 1 h, $LiAlH_4$ initial phase remains unchanged. According to this outcome and the findings of Sazelee et al. [15] and Balema et al. [51], $LiAlH_4$ was stable even after being subjected to ball milling. Figure 6c shows the XRD pattern of the $LiAlH_4$–10 wt% $TiSiO_4$ composite. In addition to the majority peaks of $LiAlH_4$, there is a new peak corresponding to the Al for the $TiSiO_4$-doped $LiAlH_4$ after 1 h milling. The appearance of Al peaks indicates that with the presence of $TiSiO_4$, hydrogen is slightly released from $LiAlH_4$ after milling (Equation (1)). However, the peaks that correspond to Li_3AlH_6 could not be detected in this pattern. Additionally, due to the small amount of $TiSiO_4$ used or the fact that $TiSiO_4$ became amorphous after 1 h of the milling process, the peaks of $TiSiO_4$ could not be detected with an XRD pattern [39,49,52].

Figure 7 depicts the FTIR spectrum used to investigate the effect of $TiSiO_4$ as a catalyst on the $LiAlH_4$ infrared spectroscopy band and to confirm the presence of Li_3AlH_6 in the $TiSiO_4$-doped $LiAlH_4$ sample after milling. In the previous studies [15,37,53], $LiAlH_4$ was represented by peaks with two bending modes between 800 and 900 cm^{-1} and two stretching modes between 1600 and 1800 cm^{-1}. Figure 7a,b show these peaks in the as-obtained and post-milled $LiAlH_4$ samples. After 1 h of milling (Figure 7c), a new peak at 1403 cm^{-1} was discovered in the $TiSiO_4$-doped $LiAlH_4$ sample. This new peak corresponds to the Al–H stretching mode of Li_3AlH_6. Although the peak of Li_3AlH_6 could not be detected in the XRD pattern (Figure 6c), the appearance of the Al–H stretching mode of

Li_3AlH_6 in the FTIR result proves that the $TiSiO_4$-doped $LiAlH_4$ sample slightly released hydrogen during the milling process (Equation (1)).

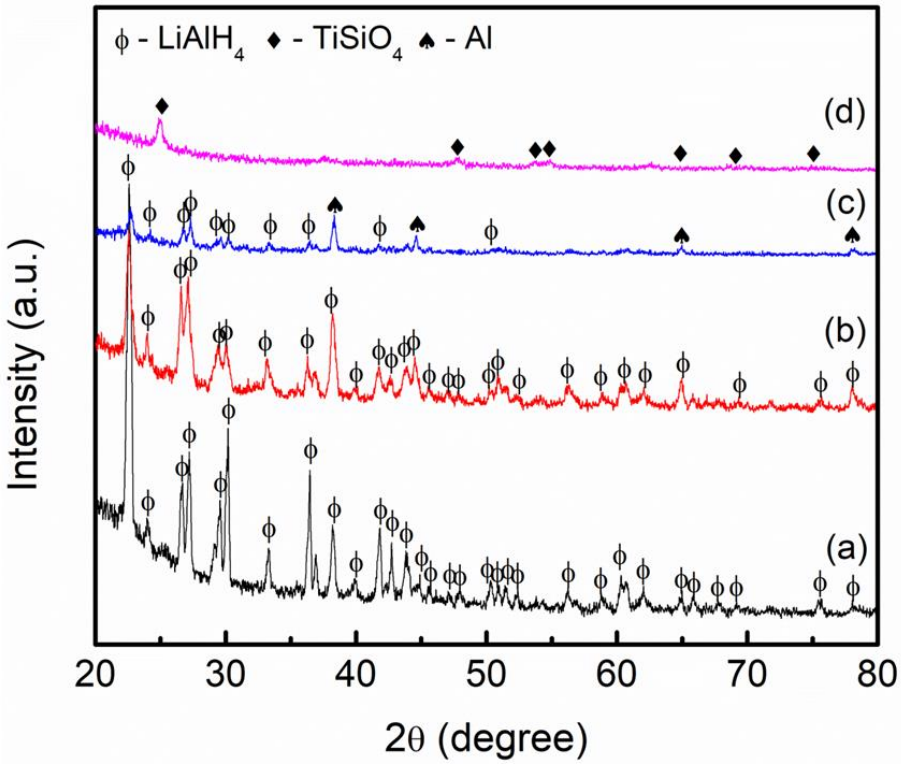

Figure 6. XRD results of (**a**) as-obtained $LiAlH_4$, (**b**) post-milled $LiAlH_4$, (**c**) $LiAlH_4$ added with 10 wt% of $TiSiO_4$, and (**d**) as-obtained $TiSiO_4$.

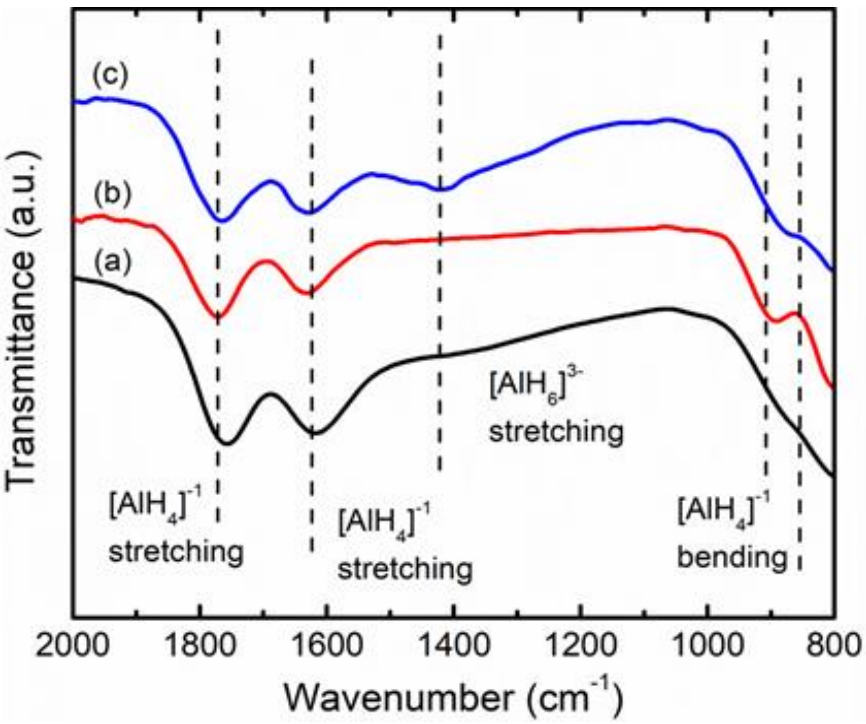

Figure 7. FTIR pattern of the (**a**) as-obtained $LiAlH_4$, (**b**) post-milled $LiAlH_4$, and (**c**) $LiAlH_4$ added with 10 wt% of $TiSiO_4$.

The XRD analysis helped to identify the catalytic and reaction mechanism behind the improvement of the dehydrogenation properties of $TiSiO_4$-added $LiAlH_4$. Figure 8 shows the results of 10 wt% and 20 wt% $TiSiO_4$-added $LiAlH_4$ composites after the dehydrogenation process at 250 °C. Due to the small amount of catalyst used, it may be challenging to identify the active species in the 10 wt% $TiSiO_4$-added $LiAlH_4$, so 20 wt% $TiSiO_4$ was added to $LiAlH_4$. The presence of the Al and LiH peaks in both samples (Figure 8a) indicates that $LiAlH_4$ has been completely dehydrogenated (Equation (2)). In addition to Al and LiH peaks, the peaks that correspond to the AlTi species can also be detected in the dehydrogenation sample. However, the peaks that correspond to the Si or Si-containing patterns could not be observed after the dehydrogenation process. This may be because the Si or Si-containing patterns were in an amorphous state. According to this research, it was hypothesized that the enhanced dehydrogenation behaviors of $LiAlH_4$ were attributed to the formation of AlTi and Si or Si-containing species. Furthermore, there were no new peaks found in the XRD patterns of the desorbed 20 wt% $TiSiO_4$-added $LiAlH_4$ composite (Figure 8b), which are similar to those of the 10 wt% $TiSiO_4$-added $LiAlH_4$ composite (Figure 8a). The peak of Al, LiH, and AlTi did not change, and no other patterns were discovered in the dehydrogenation composite, possibly because these patterns were in an amorphous state when the dehydrogenation process was complete.

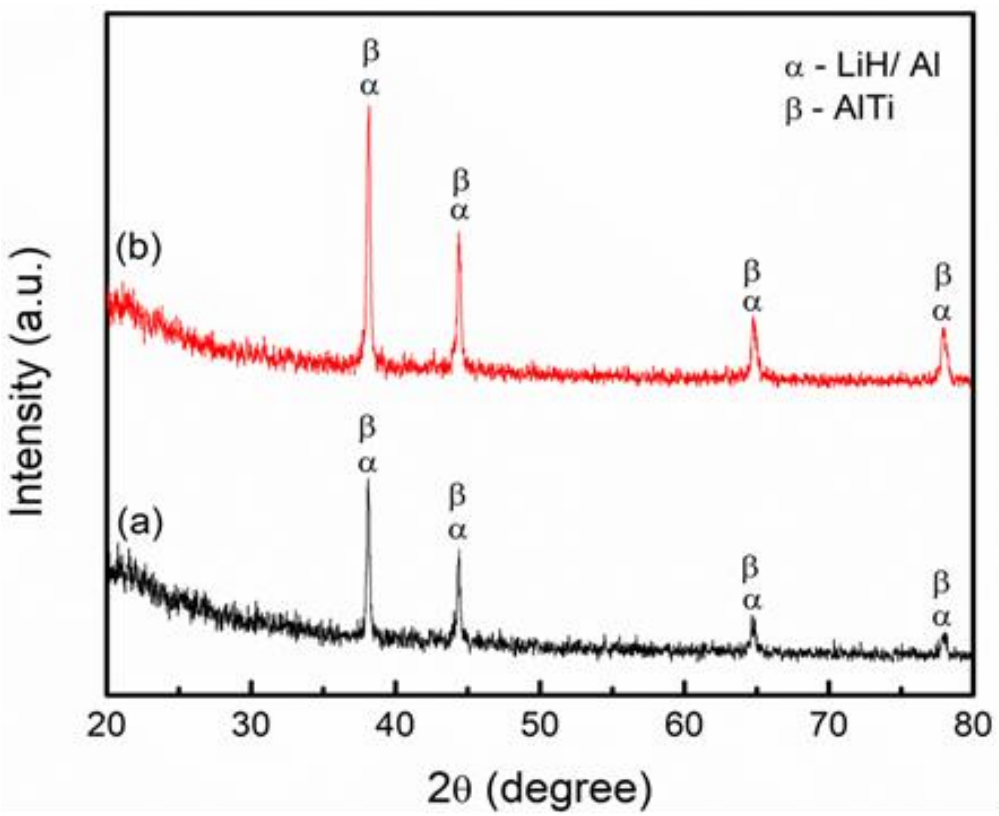

Figure 8. XRD pattern of the dehydrogenation at 250 °C of the added $LiAlH_4$ with (**a**) 10 wt% and (**b**) 20 wt% of $TiSiO_4$.

Previous studies have shown that the *in-situ* emergence of AlTi helps to improve the dehydrogenation behavior of $LiAlH_4$ [39,49,54]. Strong surface reactions between the Ti atom and $LiAlH_4$ caused a reduction in the H binding energy. The correlation between the charge transfer change between Al and H and the rapid kinetic efficiency of $LiAlH_4$ may explain the decrease in binding energy. Although the Si or Si-containing phase was not found, these species likewise play a particular role in enhancing the dehydrogenation behavior of $LiAlH_4$. For example, the Si-containing species have been proven to play a significant role in enhancing the hydrogen storage properties of MgH_2 [55]. Another study

proved that SiC could enhance the hydrogen storage properties of MgH_2 by reducing grain size and increasing defect concentration in MgH_2 particles [56,57]. However, more research is still needed, such as using high-resolution transmission electron microscopy and X-ray photoelectron spectroscopy to clarify the exact catalytic role of $TiSiO_4$ on the hydrogen storage properties of $LiAlH_4$.

4. Conclusions

In conclusion, the addition of $TiSiO_4$ improved the dehydrogenation properties of $LiAlH_4$. The introduction of $TiSiO_4$ to $LiAlH_4$ reduced the dehydrogenation temperatures for the first and second stages (start decomposing at 92 °C and 128 °C, respectively). Dehydrogenation kinetic analysis at 90 °C revealed that after 2 h, the $TiSiO_4$-added $LiAlH_4$ composite was able to liberate more hydrogen (about 6.00 wt%) than the undoped $LiAlH_4$ composite (less than 1.00 wt%). The E_A for hydrogen liberated from $LiAlH_4$ was reduced after $TiSiO_4$ was added. According to the Kissinger equation, the E_A for hydrogen liberated in the two-step dehydrogenation of post-milled $LiAlH_4$ was 103 and 115 kJ/mol, respectively. The E_A were lowered to 68 and 77 kJ/mol, respectively, after milling $LiAlH_4$ with 10 wt% of $TiSiO_4$. The addition of 10 wt% of $TiSiO_4$ also caused the $LiAlH_4$ particles to shrink and become less aggregated. According to the XRD results, $TiSiO_4$ significantly enhanced the dehydrogenation properties of $LiAlH_4$ by forming active AlTi and Si-containing species during the heating process.

Author Contributions: N.Y.Y., investigations, formal analysis, and writing—original draft preparation; N.A.A., writing—review and editing; N.S., writing—review and editing; M.I., supervision, writing—original draft preparation. All authors have read and agreed to the published version of the manuscript.

Funding: This research was funded by the Universiti Malaysia Terengganu through Golden Goose Research Grant (GGRG) (VOT 55190).

Institutional Review Board Statement: Not applicable.

Informed Consent Statement: Not applicable.

Data Availability Statement: The data presented in this study are available on request from the corresponding author.

Acknowledgments: Universiti Malaysia Terengganu is fully acknowledged for supporting this study through Golden Goose Research Grant (GGRG) (VOT 55190). N.A.A. and N.S. are grateful for the scholarship provided by Universiti Malaysia Terengganu (SIPP and BUMT).

Conflicts of Interest: The authors declare no conflict of interest.

References

1. Ye, Y.; Lu, J.; Ding, J.; Wang, W.; Yan, J. Numerical simulation on the storage performance of a phase change materials based metal hydride hydrogen storage tank. *Appl. Energy* **2020**, *278*, 115682. [CrossRef]
2. Huang, Y.; Cheng, Y.; Zhang, J. A review of high density solid hydrogen storage materials by pyrolysis for promising mobile applications. *Ind. Eng. Chem. Res.* **2021**, *60*, 2737–2771. [CrossRef]
3. Rivard, E.; Trudeau, M.; Zaghib, K. Hydrogen storage for mobility: A review. *Materials* **2019**, *12*, 1973. [CrossRef]
4. Moore, J.; Shabani, B. A critical study of stationary energy storage policies in Australia in an international context: The role of hydrogen and battery technologies. *Energies* **2016**, *9*, 674. [CrossRef]
5. Schlapbach, L.; Züttel, A. Hydrogen-storage materials for mobile applications. *J. Nat.* **2001**, *414*, 353–358. [CrossRef] [PubMed]
6. Mustafa, N.S.; Yahya, M.S.; Itam Sulaiman, N.N.; Yap, F.A.H.; Ismail, M. Enhanced the hydrogen storage properties and reaction mechanisms of $4MgH_2$+ $LiAlH_4$ composite system by addition with TiO_2. *Int. J. Energy Res.* **2021**, *45*, 21365–21374. [CrossRef]
7. Salehabadi, A.; Umar, M.F.; Ahmad, A.; Ahmad, M.I.; Ismail, N.; Rafatullah, M. Carbon-based nanocomposites in solid-state hydrogen storage technology: An overview. *Int. J. Energy. Res.* **2020**, *44*, 11044–11058. [CrossRef]
8. Egeland-Eriksen, T.; Hajizadeh, A.; Sartori, S. Hydrogen-based systems for integration of renewable energy in power systems: Achievements and perspectives. *Int. J. Hydrog. Energy* **2021**, *46*, 31963–31983. [CrossRef]
9. DOE Technical Targets for Onboard Hydrogen Storage for Light-Duty Vehicles. Available online: https://www.energy.gov/eere/fuelcells/doe-technical-targets-onboard-hydrogen-storage-light-duty-vehicles (accessed on 19 February 2023).
10. Aziz, M.; Wijayanta, A.T.; Nandiyanto, A.B.D. Ammonia as effective hydrogen storage: A review on production, storage and utilization. *Energies* **2020**, *13*, 3062. [CrossRef]

11. Ouyang, L.; Liu, F.; Wang, H.; Liu, J.; Yang, X.-S.; Sun, L.; Zhu, M. Magnesium-based hydrogen storage compounds: A review. *J. Alloys Compd.* **2020**, *832*, 154865. [CrossRef]
12. Ouyang, L.; Chen, K.; Jiang, J.; Yang, X.-S.; Zhu, M. Hydrogen storage in light-metal based systems: A review. *J. Alloy. Compd.* **2020**, *829*, 154597. [CrossRef]
13. Ali, N.A.; Ismail, M. Advanced hydrogen storage of the Mg–Na–Al system: A review. *J. Magnes. Alloy* **2021**, *9*, 1111–1122. [CrossRef]
14. Ali, N.A.; Sazelee, N.A.; Ismail, M. An overview of reactive hydride composite (RHC) for solid-state hydrogen storage materials. *Int. J. Hydrog. Energy* **2021**, *46*, 31674–31698. [CrossRef]
15. Sazelee, N.A.; Yahya, M.S.; Idris, N.H.; Din, M.M.; Ismail, M. Desorption properties of $LiAlH_4$ doped with $LaFeO_3$ catalyst. *Int. J. Hydrog. Energy* **2019**, *44*, 11953–11960. [CrossRef]
16. Ali, N.A.; Yahya, M.S.; Mustafa, N.S.; Sazelee, N.A.; Idris, N.H.; Ismail, M. Modifying the hydrogen storage performances of $NaBH_4$ by catalyzing with $MgFe_2O_4$ synthesized via hydrothermal method. *Int. J. Hydrog. Energy* **2019**, *44*, 6720–6727. [CrossRef]
17. Halim Yap, F.A.; Ali, N.A.; Idris, N.H.; Ismail, M. Catalytic effect of $MgFe_2O_4$ on the hydrogen storage properties of Na_3AlH_6–$LiBH_4$ composite system. *Int. J. Hydrog. Energy* **2018**, *43*, 20882–20891. [CrossRef]
18. Juahir, N.; Mustafa, N.S.; Yap, F.A.H.; Ismail, M. Study on the hydrogen storage properties and reaction mechanism of $NaAlH_4$–$Mg(BH_4)_2$ (2:1) with and without TiF_3 additive. *Int. J. Hydrog. Energy* **2015**, *40*, 7628–7635. [CrossRef]
19. Sazelee, N.A.; Yahya, M.S.; Ali, N.A.; Idris, N.H.; Ismail, M. Enhancement of dehydrogenation properties in $LiAlH_4$ catalysed by $BaFe_{12}O_{19}$. *J. Alloys Compd.* **2020**, *835*, 155183. [CrossRef]
20. Zheng, S.; Fang, F.; Zhou, G.; Chen, G.; Ouyang, L.; Zhu, M.; Sun, D. Hydrogen storage properties of space-confined $NaAlH_4$ nanoparticles in ordered mesoporous silica. *Chem. Mater.* **2008**, *20*, 3954–3958. [CrossRef]
21. Sigma-Aldrich. Available online: https://www.sigmaaldrich.com/MY/en/campaigns/connected-lab-instrumentation (accessed on 20 February 2023).
22. Ahmad, M.A.N.; Sazelee, N.A.; Ali, N.A.; Ismail, M. Enhancing the dehydrogenation properties of $LiAlH_4$ using K_2NiF_6 as additive. *Int. J. Hydrog. Energy* **2022**, *47*, 24843–24851. [CrossRef]
23. Fu, J. Advanced Doping Techniques and Dehydrogenation Properties of Transition Metal-Doped $LiAlH_4$ for Fuel Cell Systems. Ph.D Thesis, Dresden University of Technology, Dresden, Germany, 2015.
24. Orimo, S.-I.; Nakamori, Y.; Eliseo, J.R.; Züttel, A.; Jensen, C.M. Complex hydrides for hydrogen storage. *Chem. Rev.* **2007**, *107*, 4111–4132. [CrossRef]
25. Liu, Y.; Liang, C.; Zhou, H.; Gao, M.; Pan, H.; Wang, Q. A novel catalyst precursor K_2TiF_6 with remarkable synergetic effects of K, Ti and F together on reversible hydrogen storage of $NaAlH_4$. *Chem. Commun.* **2011**, *47*, 1740–1742. [CrossRef]
26. Andreasen, A.; Vegge, T.; Pedersen, A.S. Dehydrogenation kinetics of as-received and ball-milled $LiAlH_4$. *J. Solid State Chem.* **2005**, *178*, 3672–3678. [CrossRef]
27. Liu, S.-S.; Sun, L.-X.; Zhang, Y.; Xu, F.; Zhang, J.; Chu, H.-L.; Fan, M.Q.; Zhang, T.; Song, X.Y.; Grolier, J.P. Effect of ball milling time on the hydrogen storage properties of TiF_3-doped $LiAlH_4$. *Int. J. Hydrog. Energy* **2009**, *34*, 8079–8085. [CrossRef]
28. Liu, X.; McGrady, G.S.; Langmi, H.W.; Jensen, C.M. Facile cycling of Ti-doped $LiAlH_4$ for high performance hydrogen storage. *J. Am. Chem. Soc.* **2009**, *131*, 5032–5033. [CrossRef] [PubMed]
29. Li, Z.; Li, P.; Wan, Q.; Zhai, F.; Liu, Z.; Zhao, K.; Wang, L.; Lü, S.; Zou, L.; Qu, X.; et al. Dehydrogenation improvement of $LiAlH_4$ catalyzed by Fe_2O_3 and Co_2O_3 nanoparticles. *J. Phys. Chem. C* **2013**, *117*, 18343–18352. [CrossRef]
30. Resan, M.; Hampton, M.D.; Lomness, J.K.; Slattery, D.K. Effects of various catalysts on hydrogen release and uptake characteristics of $LiAlH_4$. *Int. J. Hydrog. Energy* **2005**, *30*, 1413–1416. [CrossRef]
31. Balema, V.P.; Wiench, J.W.; Dennis, K.W.; Pruski, M.; Pecharsky, V.K. Titanium catalyzed solid-state transformations in $LiAlH_4$ during high-energy ball-milling. *J. Alloys Compd.* **2001**, *329*, 108–114. [CrossRef]
32. Shenglin, L.; Qiuhua, M.; Xueping, Z.; Xin, F.; Guo, X.; Jiaojiao, Z. Influences of Y_2O_3 doping on hydrogen release property of $LiAlH_4$. *Rare Metal Mat. Eng.* **2014**, *43*, 287–290. [CrossRef]
33. Cao, Z.; Ma, X.; Wang, H.; Ouyang, L. Catalytic effect of $ScCl_3$ on the dehydrogenation properties of $LiAlH_4$. *J. Alloys Compd.* **2018**, *762*, 73–79. [CrossRef]
34. Varin, R.A.; Zbroniec, L. Fast and slow dehydrogenation of ball milled lithium alanate ($LiAlH_4$) catalyzed with manganese chloride ($MnCl_2$) as compared to nanometric nickel catalyst. *J. Alloys Compd.* **2011**, *509*, S736–S739. [CrossRef]
35. Sazelee, N.A.; Ismail, M. Recent advances in catalyst-enhanced $LiAlH_4$ for solid-state hydrogen storage: A review. *Int. J. Hydrog. Energy* **2021**, *46*, 9123–9141. [CrossRef]
36. Zhai, F.; Li, P.; Sun, A.; Wu, S.; Wan, Q.; Zhang, W.; Li, Y.; Cui, L.; Qu, X. Significantly improved dehydrogenation of $LiAlH_4$ destabilized by $MnFe_2O_4$ nanoparticles. *J. Phys. Chem. C* **2012**, *116*, 11939–11945. [CrossRef]
37. Ismail, M.; Zhao, Y.; Yu, X.; Nevirkovets, I.; Dou, S. Significantly improved dehydrogenation of $LiAlH_4$ catalysed with TiO_2 nanopowder. *Int. J. Hydrog. Energy* **2011**, *36*, 8327–8334. [CrossRef]
38. Xuanhui, Q.; Ping, L.; Zhang, L.; Ahmad, M. Hydrogen sorption improvement of $LiAlH_4$ catalyzed by Nb_2O_5 and Cr_2O_3 nanoparticles. *J. Phys. Chem. C* **2011**, *115*, 13088–13099.
39. Ismail, M.; Ali, N.A.; Sazelee, N.A.; Suwarno, S. Catalytic effect of Al_2TiO_5 on the dehydrogenation properties of $LiAlH_4$. *Int. J. Hydrog. Energy* **2022**, *47*, 31903–31910. [CrossRef]

40. Ismail, M.; Sazelee, N.A.; Ali, N.A.; Suwarno, S. Catalytic effect of $SrTiO_3$ on the dehydrogenation properties of $LiAlH_4$. *J. Alloys Compd.* **2021**, *855*, 157475. [CrossRef]
41. Li, L.; An, C.; Wang, Y.; Xu, Y.; Qiu, F.; Wang, Y.; Jiao, L.; Yuan, H. Enhancement of the H_2 desorption properties of $LiAlH_4$ doping with $NiCo_2O_4$ nanorods. *Int. J. Hydrog. Energy* **2014**, *39*, 4414–4420. [CrossRef]
42. Liu, S.-S.; Li, Z.-B.; Jiao, C.-L.; Si, X.-L.; Yang, L.-N.; Zhang, J.; Zhou, H.Y.; Huang, F.L.; Gabelica, Z.; Schick, C.; et al. Improved reversible hydrogen storage of $LiAlH_4$ by nano-sized TiH_2. *Int. J. Hydrog. Energy* **2013**, *38*, 2770–2777. [CrossRef]
43. Ismail, M.; Zhao, Y.; Yu, X.B.; Ranjbar, A.; Dou, S.X. Improved hydrogen desorption in lithium alanate by addition of SWCNT–metallic catalyst composite. *Int. J. Hydrog. Energy* **2011**, *36*, 3593–3599. [CrossRef]
44. Ismail, M.; Zhao, Y.; Yu, X.B.; Dou, S.X. Effects of NbF_5 addition on the hydrogen storage properties of $LiAlH_4$. *Int. J. Hydrog. Energy* **2010**, *35*, 2361–2367. [CrossRef]
45. Czujko, T.; Oleszek, E.E.; Szot, M. New aspects of MgH_2 morphological and structural changes during high-energy ball milling. *Materials* **2020**, *13*, 4550. [CrossRef]
46. Révész, Á.; Gajdics, M. Improved H-storage performance of novel Mg-based nanocomposites prepared by high-energy ball milling: A review. *Energies* **2021**, *14*, 6400. [CrossRef]
47. Varin, R.A.; Czujko, T.; Wronski, Z. Particle size, grain size and γ-MgH_2 effects on the desorption properties of nanocrystalline commercial magnesium hydride processed by controlled mechanical milling. *Nanotechnology* **2006**, *17*, 3856. [CrossRef]
48. Cai, J.; Zang, L.; Zhao, L.; Liu, J.; Wang, Y. Dehydrogenation characteristics of $LiAlH_4$ improved by in-situ formed catalysts. *J. Energy Chem.* **2016**, *25*, 868–873. [CrossRef]
49. Ali, N.A.; Ahmad, M.A.N.; Yahya, M.S.; Sazelee, N.; Ismail, M. Improved dehydrogenation properties of $LiAlH_4$ by addition of nanosized $CoTiO_3$. *Nanomaterials* **2022**, *12*, 3921. [CrossRef] [PubMed]
50. Devrim, Y.; Erkan, S.; Bac, N.; Eroglu, I. Improvement of PEMFC performance with Nafion/inorganic nanocomposite membrane electrode assembly prepared by ultrasonic coating technique. *Int. J. Hydrog. Energy* **2012**, *37*, 16748–16758. [CrossRef]
51. Balema, V.P.; Pecharsky, V.K.; Dennis, K.W. Solid state phase transformations in $LiAlH_4$ during high-energy ball-milling. *J. Alloys Compd.* **2000**, *313*, 69–74. [CrossRef]
52. Xia, Y.; Zhang, H.; Sun, Y.; Sun, L.; Xu, F.; Sun, S.; Zhang, G.; Huang, P.; Du, Y.; Wang, J.; et al. Dehybridization effect in improved dehydrogenation of $LiAlH_4$ by doping with two-dimensional Ti_3C_2. *Mater. Today Nano* **2019**, *8*, 100054. [CrossRef]
53. Rafi ud, d.; Zhang, L.; Ping, L.; Xuanhui, Q. Catalytic effects of nano-sized TiC additions on the hydrogen storage properties of $LiAlH_4$. *J. Alloy. Compd.* **2010**, *508*, 119–128. [CrossRef]
54. Zang, L.; Cai, J.; Zhao, L.; Gao, W.; Liu, J.; Wang, Y. Improved hydrogen storage properties of $LiAlH_4$ by mechanical milling with TiF_3. *J. Alloy. Compd.* **2015**, *647*, 756–762. [CrossRef]
55. Ismail, M.; Yahya, M.S.; Sazelee, N.A.; Ali, N.A.; Yap, F.A.H.; Mustafa, N.S. The effect of K_2SiF_6 on the MgH_2 hydrogen storage properties. *J. Magnes. Alloy* **2020**, *8*, 832–840. [CrossRef]
56. Ranjbar, A.; Guo, Z.; Yu, X.; Attard, D.; Calka, A.; Liu, H.-K. Effects of SiC nanoparticles with and without Ni on the hydrogen storage properties of MgH_2. *Int. J. Hydrog. Energy* **2009**, *34*, 7263–7268. [CrossRef]
57. Kurko, S.; Rašković, Ž.; Novaković, N.; Mamula, B.P.; Jovanović, Z.; Baščarević, Z.; Novaković, J.G.; Matović, L. Hydrogen storage properties of MgH_2 mechanically milled with α and β SiC. *Int. J. Hydrog. Energy* **2011**, *36*, 549–554. [CrossRef]

Disclaimer/Publisher's Note: The statements, opinions and data contained in all publications are solely those of the individual author(s) and contributor(s) and not of MDPI and/or the editor(s). MDPI and/or the editor(s) disclaim responsibility for any injury to people or property resulting from any ideas, methods, instructions or products referred to in the content.